

This is the peer reviewed version of the following article:

Radical-lanthanide ferromagnetic interaction in a TbIII bis-phthalocyaninato complex / Komijani, Dorsa; Ghirri, Alberto; Bonizzoni, Claudio; Klyatskaya, Svetlana; Moreno-Pineda, Eufemio; Ruben, Mario; Soncini, Alessandro; Affronte, Marco; Hill, Stephen. - In: PHYSICAL REVIEW MATERIALS. - ISSN 2475-9953. - 2:2(2018), pp. 1-9. [10.1103/PhysRevMaterials.2.024405]

Terms of use:

The terms and conditions for the reuse of this version of the manuscript are specified in the publishing policy. For all terms of use and more information see the publisher's website.

03/05/2026 13:51

(Article begins on next page)

Important Notice to Authors

No further publication processing will occur until we receive your response to this proof.

Attached is a PDF proof of your forthcoming article in Physical Review Materials. Your article has 9 pages and the Accession Code is **MM10060**.

Please note that as part of the production process, APS converts all articles, regardless of their original source, into standardized XML that in turn is used to create the PDF and online versions of the article as well as to populate third-party systems such as Portico, Crossref, and Web of Science. We share our authors' high expectations for the fidelity of the conversion into XML and for the accuracy and appearance of the final, formatted PDF. This process works exceptionally well for the vast majority of articles; however, please check carefully all key elements of your PDF proof, particularly any equations or tables.

Figures submitted electronically as separate files containing color appear in color in the journal.

Specific Questions and Comments to Address for This Paper

- 1 Please check "tunnel splitting ~kHz" and "tunnel splitting ~K". The meaning is not clear. Please clarify what is meant.
 - 2 Please check definition.
 - 3 Except for the term "and/or," the use of the slash is discouraged between words and abbreviations, as the meaning is ambiguous, especially in this case.
 - 4 Please check degree symbols.
 - 5 Please define "XMCD" and "RASSI-SO."
 - 6 We have remove Section VI SUPPLEMENTAL MATERIALS. Please check.
 - 7 Please check "Grant No." throughout.
 - 8 Please update.
 - 9 Please update.
- FQ:** This funding provider could not be uniquely identified during our search of the FundRef registry (or no Contract or Grant number was detected). Please check information and amend if incomplete or incorrect.
- Q:** This reference could not be uniquely identified due to incomplete information or improper format. Please check all information and amend if applicable.

Open Funder Registry: Information about an article's funding sources is now submitted to Crossref to help you comply with current or future funding agency mandates. Crossref's Open Funder Registry (<https://www.crossref.org/services/funder-registry/>) is the definitive registry of funding agencies. Please ensure that your acknowledgments include all sources of funding for your article following any requirements of your funding sources. Where possible, please include grant and award ids. Please carefully check the following funder information we have already extracted from your article and ensure its accuracy and completeness:

US National Science Foundation, DMR-1610226

Air Force Office of Scientific Research (US)

Asian Office of Research and Development, FA2386-17-1-4040

Italian Ministry of Education and Research, 2015HYFSRT, DFG-TR 88, ANR-13-BS10-0001-03

Australian Research Council (AU), DP15010325

National Science Foundation (LK), DMR-1157490

Other Items to Check

- Please note that the original manuscript has been converted to XML prior to the creation of the PDF proof, as described above. Please carefully check all key elements of the paper, particularly the equations and tabular data.
- Title: Please check; be mindful that the title may have been changed during the peer-review process.
- Author list: Please make sure all authors are presented, in the appropriate order, and that all names are spelled correctly.
- Please make sure you have inserted a byline footnote containing the email address for the corresponding author, if desired. Please note that this is not inserted automatically by this journal.
- Affiliations: Please check to be sure the institution names are spelled correctly and attributed to the appropriate author(s).
- Receipt date: Please confirm accuracy.
- Acknowledgments: Please be sure to appropriately acknowledge all funding sources.
- Hyphenation: Please note hyphens may have been inserted in word pairs that function as adjectives when they occur before a noun, as in "x-ray diffraction," "4-mm-long gas cell," and "R-matrix theory." However, hyphens are deleted from word pairs when they are not used as adjectives before nouns, as in "emission by x rays," "was 4 mm in length," and "the R matrix is tested."

Note also that Physical Review follows U.S. English guidelines in that hyphens are not used after prefixes or before suffixes: superresolution, quasiequilibrium, nanoprecipitates, resonancelike, clockwise.

- Please check that your figures are accurate and sized properly. Make sure all labeling is sufficiently legible. Figure quality in this proof is representative of the quality to be used in the online journal. To achieve manageable file size for online delivery, some compression and downsampling of figures may have occurred. Fine details may have become somewhat fuzzy, especially in color figures. Figures to be published in color online will appear in color on these proofs if viewed on a color monitor or printed on a color printer.
- Please check to ensure that reference titles are given as appropriate.
- Overall, please proofread the entire *formatted* article very carefully. The redlined PDF should be used as a guide to see changes that were made during copyediting. However, note that some changes to math and/or layout may not be indicated.

Ways to Respond

- **Web:** If you accessed this proof online, follow the instructions on the web page to submit corrections.
- **Email:** Send corrections to prmproofs@aptaracorp.com
Subject: **MM10060** proof corrections
- **Fax:** Return this proof with corrections to +1.703.791.1217. Write **Attention: PRM Project Manager** and the Article ID, **MM10060**, on the proof copy unless it is already printed on your proof printout.

Radical-lanthanide ferromagnetic interaction in a Tb^{III} bis-phthalocyaninato complex

Dorsa Komijani,^{1,2} Alberto Ghirri,³ Claudio Bonizzi,^{3,4} Svetlana Klyatskaya,⁵ Eufemio Moreno-Pineda,⁵ Mario Ruben,⁵ Alessandro Soncini,⁶ Marco Affronte,^{3,4,*} and Stephen Hill^{1,2,†}

¹Department of Physics, Florida State University, Tallahassee, Florida 32306, USA

²National High Magnetic Field Laboratory, Tallahassee, Florida 32310, USA

³CNR-Instituto Nanoscienze, via G. Campi 213A, 41125 Modena, Italy

⁴Dipartimento di Scienze Fisiche, Informatiche e Matematiche, Università di Modena e Reggio Emilia, via G. Campi 213A, 41125 Modena, Italy

⁵Karlsruhe Institute of Technology (KIT), Institute of Nanotechnology, Eggenstein-Leopoldshafen, Germany

⁶School of Chemistry, The University of Melbourne, 3010 Victoria, Australia



(Received 27 December 2017; published xxxxxx)

Recent studies have highlighted the importance of organic ligands in the field of molecular spintronics, via which delocalized electron-spin density can mediate magnetic coupling to otherwise localized $4f$ moments of lanthanide ions, which show tremendous potential for single-molecule device applications. To this end, high-field/high-frequency electron paramagnetic resonance (EPR) spectroscopy is employed to study a neutral terbium bis-phthalocyaninato metalorganic complex, $[\text{TbPc}_2]^0$, with the aim of understanding the magnetic interaction between the Ising-like moment of the lanthanide ion and the unpaired spin density on the coordinating organic radical ligand. The measurements were performed on a previously unknown $[\text{TbPc}_2]^0$ structural phase crystallizing in the $Pnma$ space group. EPR measurements on powder samples of $[\text{TbPc}_2]^0$ reveal an anisotropic spectrum, which is attributed to the spin- $\frac{1}{2}$ radical coupled weakly to the EPR-silent Tb^{III} ion. Extensive double-axis rotation studies on a single crystal reveal two independent spin- $\frac{1}{2}$ signals with differently oriented (albeit identical) uniaxial g -tensors, in complete agreement with x-ray structural studies that indicate two molecular orientations within the unit cell. The easy-axis nature of the radical EPR spectra thus reflects the coupling to the Ising-like Tb^{III} moment. This is corroborated by studies of the isostructural $[\text{YPc}_2]^0$ analog (where Y is nonmagnetic yttrium), which gives a completely isotropic radical EPR signal. The experimental results for the terbium complex are well explained on the basis of an effective model that introduces a weak ferromagnetic Heisenberg coupling between an isotropic spin- $\frac{1}{2}$ and an anisotropic spin-orbital moment, $J = 6$, that mimics the known, strong easy-axis Tb \cdots Pc₂ crystal-field interaction.

DOI: [10.1103/PhysRevMaterials.00.004400](https://doi.org/10.1103/PhysRevMaterials.00.004400)

I. INTRODUCTION

The study of electron delocalization involving spin-bearing (radical) ligands coordinated to metal ions is relevant to a wide range of research topics, including organic electronics, photovoltaics, and catalysis, as well as many important biological processes and biomedical applications [1–4]. This subject also became of interest within the molecular magnetism and nanomagnetism communities, given the demonstration that radical-bearing ligands can mediate strong exchange interactions between otherwise magnetically isolated lanthanide (Ln) ions, resulting in a leap forward in the development of spin-chain systems [5–7] and so-called single-molecule magnets (SMMs) [8–10]—molecules that can be magnetized below a characteristic blocking temperature T_B . More recently, it has been recognized that delocalized electrons in organic radicals play a key role in mediating coupling between lanthanide magnetic moments and magnetic surfaces [11,12], or to conduction electrons in spintronic devices [13,14]. Moreover,

charge transport through organic ligands provides a means of addressing electron and nuclear quantum states associated with lanthanide qubits integrated into single-molecule spin transistors [15–17].

Although electron paramagnetic resonance (EPR) investigations have previously been employed to study Ln-radical systems [18,19], transitions are typically silent or forbidden at the low microwave frequencies of commercial EPR spectrometers; this is due primarily to the large moment and strong crystal-field anisotropy of most lanthanides, resulting in an Ising-type coupling to the radical and appreciable zero-field gaps associated with allowed magnetic dipole transitions. Consequently, the few EPR investigations targeted directly at understanding Ln-radical interactions have been performed on homebuilt high-field instruments [20,21]. Motivated by the potential use of Tb^{III}-bis-phthalocyaninato (TbPc₂) sandwich complexes in spintronic devices and quantum information processing applications, as well as for magnetic interfaces, we set out to explore whether the magnetic properties of the highly anisotropic and sizable Tb^{III} moment can be probed via its coupling to a nearby radical through the use of high-frequency microwave techniques. To this end, we report single-crystal and powder high-field EPR (HF-EPR) measurements on a neutral $[\text{TbPc}_2]^0$

*marco.affronte@unimore.it

†shill@magnet.fsu.edu

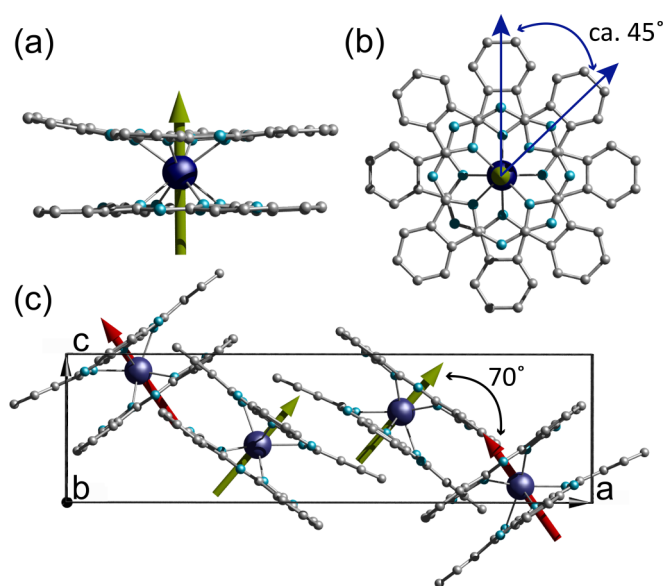


FIG. 1. Molecular structure and packing of $[\text{TbPc}_2]^0$: (a) side view; (b) top view; and (c) packing diagram of the molecules in the unit cell, displaying two magnetically inequivalent sets of molecules with their easy axes (red/green arrows) tilted approximately 70° with respect to each other. Color scheme: Tb, purple; N, blue; C, gray; H atoms have been omitted for clarity.

complex for which the organic bis-phthalocyaninato ligand is open shell; i.e., it carries an unpaired electron. A highly anisotropic EPR signal can be attributed to the radical, suggesting an appreciable interaction with the Ising-like Tb^{III} ion.

As reported by Ishikawa *et al.* in 2003 [22], the organometallic $[\text{TBA}]^+[\text{LnPc}_2]^-$ complex [$\text{Ln} = \text{Tb}, \text{Dy}$, and $\text{TBA}^+ = \text{N}(\text{C}_4\text{H}_9)_4^+$] was the first example of a SMM containing just a single metal ion, in this case sandwiched between the two organic Pc ligands. Oxidation of $[\text{Tb}(\text{Pc})_2]^-$ results in $[\text{TbPc}_2]^0$ (**1**), a neutral complex with an unpaired electron now delocalized over the two Pc rings (Fig. 1) [23]. The Tb^{III} ion has a spin-orbit coupled angular momentum ground state of $J = 6$ ($L = 3, S = 3$), with the lowest (approximately degenerate) substates as $m_J = \pm 6$ derived on the basis of fits to ^1He NMR paramagnetic shifts and temperature-dependent magnetic susceptibility [24]. The easy axis of the terbium ion is defined by the C_4 symmetry axis of the molecule, i.e., perpendicular to the planes of the Pc rings [Fig. 1(a)]. Meanwhile, the next excited states ($m_J = \pm 5$) lie more than 400 cm^{-1} above the $m_J = \pm 6$ states and are, thus, not populated at low temperatures [24]. This large separation between the $m_J = \pm 6$ and ± 5 substates is a direct consequence of the strong axial nature of the crystal field imposed by the Pc_2 ligands on the nonspherical $4f$ electron density associated with the Tb^{III} ion. This, in turn, results in highly pure $m_J = \pm 6$ states (tunnel splitting $\sim \text{kHz}$) [25]. Thus, in contrast to recent studies of a similar Ho^{III} compound with a $4f$ electron density that is closer to spherical (tunnel splitting $\sim \text{K}$) [26], EPR transitions between the ground substates in **1** cannot be observed directly via EPR. However, the unpaired spin on the ligand provides an indirect way to spectroscopically probe the Tb^{III} ion and its coupling to the radical.

II. EXPERIMENTAL DETAILS

The investigated complexes, $[\text{TbPc}_2]^0$ (**1**) and isostructural $[\text{YPc}_2]^0$ (**2**), where Y is nonmagnetic, were synthesized according to previously established procedures [27]. Continuous wave (cw) HF-EPR measurements were first performed at low temperatures on a finely ground powder of **1** and **2** in the frequency range from 52 to 412 GHz. A transmission-type spectrometer was employed for these purposes in which microwaves are propagated through cylindrical light pipes into (and out of) a variable-flow He cryostat situated within the bore of a 15/17 T superconducting magnet [28]. Microwaves were generated using a phase-locked source (Virginia Diode) operating at a base frequency of 12–14 GHz followed by a chain of multipliers. The returned microwave signal was recorded using magnetic field modulation and a liquid He cooled InSb bolometer. The fine powders were pressed into polyethylene cups using a Teflon stopper to prevent mobilization in the presence of the externally applied magnetic field.

Single-crystal measurements were carried out on **1** using a cavity perturbation technique, employing a millimeter-wave vector network analyzer (MVNA) in combination with various microwave sources and detectors [29,30]. Field-swept HF-EPR spectra were recorded in a 9-5-1 T superconducting vector magnet, at fixed frequencies in the 50–104 GHz range. A variable-flow He gas cryostat was again used for temperature control. A single needle-shaped crystal (approximate dimensions $1.5 \times 0.4 \times 0.4 \text{ mm}^3$) was selected for study, and subsequently mounted horizontally on the base plate of a vertical cylindrical resonator. Due to the low-symmetry space group of **1** (see below), the unit cell axes do not project in a simple way onto the crystal shape. Consequently, extensive angle-dependent studies were first performed via *in situ* double-axis rotation: the 9-5 T component of the vector field was employed to rotate the applied field in the polar angle θ in 10° increments ($\theta = 0^\circ$ corresponds to the field being parallel to the vertical cylindrical axis of the resonator); meanwhile, the azimuthal angle ϕ was varied in 20° increments by physically rotating the resonator about its cylindrical axis. EPR spectra were then recorded at 65.5 GHz and 2 K over a 180° range in θ , for 12 azimuthal planes of rotation in ϕ , i.e., a full 4π steradians. Frequency-dependent measurements were subsequently performed at field orientations parallel to the deduced magnetic symmetry axes. All simulations were performed using the program EASYSFIN [31].

III. RESULTS

Structural characterization. Single-crystal x-ray diffraction studies of **1** and **2** show that the molecules crystallize in an orthorhombic unit cell (see the Supplemental Material [32]). The crystals were obtained via slow vapor diffusion of dichloromethane into a solution of 1,1,2,2-tetrachloroethane containing the complex [27]. Interestingly, concentrations above 4.5 mM yield crystals in the $P2_12_12_1$ space group, while lower concentrations lead to the $Pnma$ space group. In the $P2_12_12_1$ space group, a total of four distinct (differently oriented) molecules are contained within the unit cell while, in the $Pnma$ space group, only two independent molecules are found. Due to these observations, we focus here exclusively

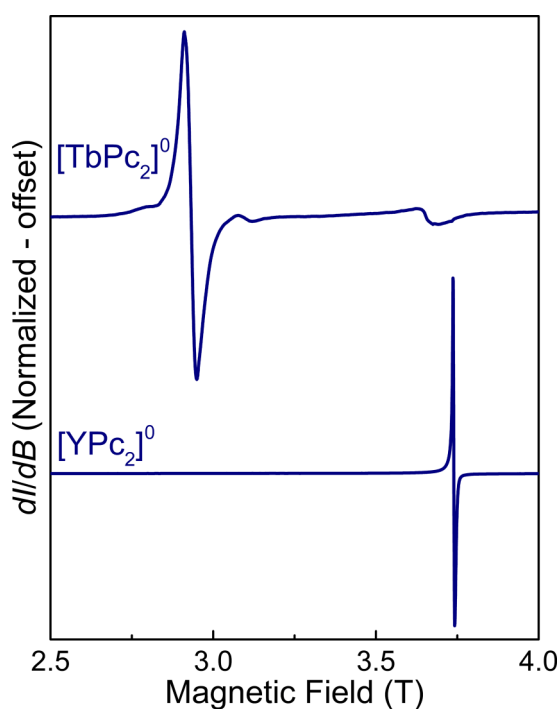


FIG. 2. Powder EPR spectra collected on samples of **1** and **2** at a frequency of 104.8 GHz and a temperature of 5 K; the data were recorded in derivative mode, dI/dB (I = absorption intensity).

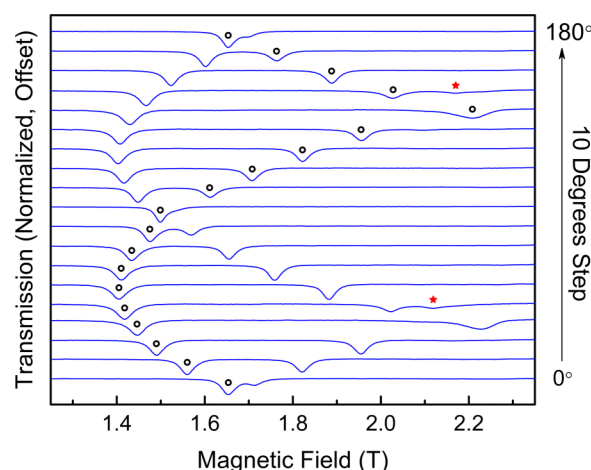


FIG. 3. Angle-dependent EPR spectra for a single crystal of **1** for a full 180° rotation of θ (with $\phi = 120^\circ$), collected at a frequency of 65.5 GHz and temperature of 2 K; the dips in transmission correspond to the resonances. The green circles denote resonances for one of the two molecular orientations: note the smooth variation with angle from the cusplike maximum (at ~ 2.2 T), through a broad minimum (at ~ 1.4 T), with an overall 180° periodicity. An additional weak resonance is observed at two of the angles (marked with *), which we explain in Sec. IV.

162 on the complexes crystallizing in the $Pnma$ space group be-
 163 cause they are expected to exhibit less complex spectroscopic
 164 behavior.

165 We describe only the structural characteristics of **1**, as it
 166 exhibits the most interesting spectroscopic properties. Single-
 167 crystal x-ray studies reveal only half of the molecule residing
 168 in the asymmetric unit, with two differently oriented molecules
 169 and a total of four molecules within the unit cell [Fig. 1(c)].
 170 The two spatially different molecules are related by a rotation
 171 about the crystallographic b axis of $\sim 70^\circ$. Locally, the Tb^{III} ion
 172 resides in a very symmetric environment. The eight isoindole
 173 nitrogens of the Pc_2 ligands impose a square antiprismatic
 174 coordination geometry on the Tb^{III} ion, with the two Pc ligands
 175 arranged above and below in a near perfect staggered configura-
 176 tion. The average distance to the eight coordinating nitrogens
 177 is 2.4186(2) Å, while the mean distance to the planes of the
 178 Pc ligands is 1.4064(1) Å. Note that the distances observed
 179 here for the neutral $[\text{TbPc}_2]^0$ (**1**) are slightly shorter than those
 180 reported for the negatively charged analog, $\text{TBA}^+[\text{TbPc}_2]^-$
 181 [33], where the $\langle \text{Tb} \cdots \text{N} \rangle$ and $\langle \text{Tb} \cdots \text{Pc} \rangle$ distances are
 182 2.8245(3) and 1.4122(3) Å, respectively. The average twist
 183 angle between the two Pc moieties is 45° [Fig. 1(b)], compared
 184 to 44.1° for the $\text{TBA}^+[\text{TbPc}_2]^-$ analog. Therefore, the Tb^{III} ion
 185 of **1** experiences a near ideal local D_{4d} crystal-field symmetry.

186 *Spectroscopy.* EPR spectra collected on powder samples of
 187 **1** and **2**, at a frequency of 104.8 GHz and a temperature of
 188 5 K, are shown in Fig. 2. The $[\text{YPc}_2]^0$ complex (**2**) displays
 189 a sharp signal at ~ 3.75 T (peak-to-peak linewidth ~ 5 mT),
 190 corresponding to an isotropic Landé g factor of 2.003(1)
 191 that can be ascribed to the $\text{spin-}\frac{1}{2}$ radical; the first derivative
 192 line shape results from the lock-in detection of the field

193 modulated signal, dI/dB , where I represents the absorption
 194 intensity. By contrast, the EPR spectrum of $[\text{TbPc}_2]^0$ (**1**) shows
 195 a significantly broader spectrum, with two prominent features
 196 spanning all the way from the strong first derivative signal
 197 at 2.93 T (peak-to-peak linewidth ~ 37 mT) to the weaker
 198 asymmetric dip at the isotropic $g = 2.00$ position (~ 3.75 T).
 199 Such a powder spectrum is typical for a species experiencing an
 200 axial magnetic anisotropy, with the two features corresponding
 201 to the parallel and perpendicular components. It is worth
 202 noting that the EPR spectrum of the charged $\text{TBA}^+[\text{TbPc}_2]^-$
 203 derivative, for which the radical is absent, does not show any
 204 visible EPR transition. This confirms a strong axiality and
 205 negligible mixing within the ground $m_J = \pm 6$ substates of
 206 the Tb^{III} ion, such that the transition between them is strongly
 207 forbidden. Consequently, the entire spectrum recorded for the
 208 $[\text{TbPc}_2]^0$ complex is ascribable to the radical. In turn, the
 209 anisotropic nature of this spectrum provides the first indication
 210 that the radical is coupled to the Tb^{III} ion, because an isolated
 211 radical would otherwise give the same narrow spectrum as the
 212 $[\text{YPc}_2]^0$ complex.

213 Single-crystal EPR measurements were subsequently carried
 214 out on **1** in order to study the effect of the lanthanide ion on
 215 the radical in more detail. Angle-dependent spectra collected at
 216 65.5 GHz and 2 K for a full 180° rotation of θ (with $\phi = 120^\circ$)
 217 are shown in Fig. 3. Two sharp angle-dependent resonances
 218 of comparable linewidth to those observed for the pure radical
 219 (Fig. 2) are seen at essentially all angles (except at $\theta = 90^\circ$,
 220 where they merge to a single asymmetric resonance). This,
 221 together with the field dependence (*vide infra*), which ascribes
 222 g factors of ~ 2.00 to both resonances, corroborates their
 223 assignment to the $\text{spin-}\frac{1}{2}$ radicals. The fact that the separation
 224 of the parallel and perpendicular components of the 104.8 GHz
 225 powder spectrum (~ 0.82 T; see Fig. 2) is comparable to the
 226 range of the 65.5 GHz single-crystal data in Fig. 3 suggests

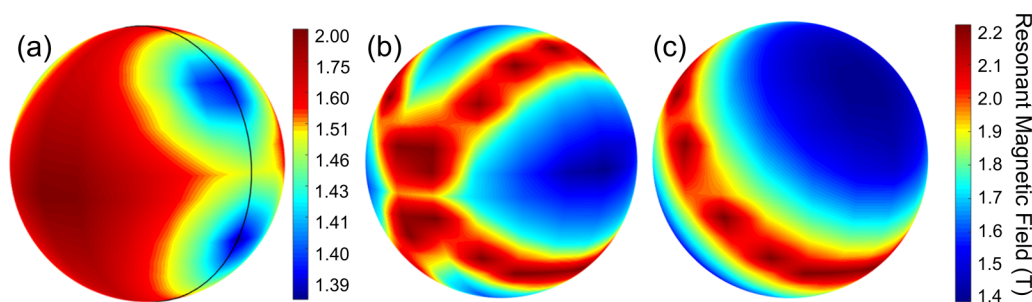


FIG. 4. 3D color maps of the positions of the lowest- (a) and highest- (b) field 65.5 GHz EPR positions, highlighting the easy (blue) and hard (red) magnetization directions of the Tb^{III} ion, respectively; the black line in (a) marks the $\phi = 120^\circ$ plane of rotation, which intersects the easy axes of the two differently oriented molecules (see Fig. 3). (c) Resonance position for one of the two molecular orientations, clearly indicating an easy-axis anisotropy. The two hard planes and easy axes are tilted $\sim 70^\circ$ with respect to each other, in excellent agreement with the orientations of the two [TbPc₂]⁰ molecules (see Fig. 1).

227 a field-independent anisotropic interaction, likely involving a
 228 coupling of the radical to the terbium ion, as the spectrum
 229 would otherwise be isotropic. Meanwhile, the fact that two
 230 EPR transitions are observed with distinct angle dependences
 231 can be attributed to the existence of two differently oriented
 232 molecules within the unit cell of compound **1** [Fig. 1(c)]. By
 233 following the evolution of the resonance positions with angle,
 234 it is straightforward to assign each one to a given molecular
 235 orientation, as seen in Fig. 3.

236 Additional data sets under the same conditions as those
 237 displayed in Fig. 3 were collected for multiple azimuthal
 238 planes of rotation. Figure 4 displays three-dimensional (3D)
 239 color maps representing these angle dependences mapped
 240 onto a complete sphere. Because there is more than one
 241 resonance for each field orientation, the data are presented in
 242 several ways, emphasizing different aspects of the magnetic
 243 anisotropy of **1**: (a) plots the position of the lowest-resonance
 244 field, highlighting the easy directions (dark blue); (b) plots
 245 the position of the highest resonance field, accentuating the
 246 hard directions (red); and (c) plots the resonance position for
 247 only one of the two molecular orientations. The color maps
 248 clearly indicate an easy-axis anisotropy for both molecular
 249 orientations; i.e., the hard directions are confined to planes,
 250 with easy directions along two axes that are orthogonal to the
 251 hard planes. Moreover, the hard planes and/or easy axes are
 252 tilted $\sim 70^\circ$ with respect to each other, in excellent agreement
 253 with the orientations of the two [TbPc₂]⁰ molecules determined
 254 from x-ray diffraction measurements [Fig. 1(c)].

255 From the above measurements, it is straightforward to locate
 256 the magnetic symmetry axes/planes for each molecular orienta-
 257 tion. In fact, the crystal was mounted within the resonator such
 258 that the $\phi = 120^\circ$ azimuthal plane approximately intersects the
 259 easy axes (and hard planes) of both orientations [see Fig. 4(a)];
 260 note that this corresponds to the situation in Fig. 3. For this
 261 plane of rotation, one can therefore define polar angles, ψ_1 and
 262 ψ_2 , that represent the alignment of the applied magnetic field
 263 with respect to the easy axes of the two molecular orientations.
 264 Such a transformation from the laboratory frame (θ, ϕ) to
 265 local coordinates (ψ_i) is illustrated in Fig. 5, which displays
 266 the ψ dependence of the resonance positions for one of the
 267 molecular orientations in Fig. 3: The easy ($\psi = 0$) and hard
 268 ($\psi = \pm 90^\circ$) directions are noted in the figure, and simulated
 269 angle dependences (*vide infra*) are superimposed on the data.

270 Figure 6 plots the frequency dependence of resonance
 271 positions for the easy ($\psi = 0$) and hard ($\psi = 90^\circ$) directions of
 272 [TbPc₂]⁰ (**1**). As noted above, the magnitude of the anisotropy,
 273 as measured by the separation of the $\psi = 0$ and 90° resonances,
 274 is field independent. Moreover, agreement between the single-
 275 crystal and powder data is good over the entire range investi-
 276 gated. Importantly, the ~ 26 -GHz zero-field intercept/gap in the
 277 spectrum cannot be explained in terms of noninteracting spin- $\frac{1}{2}$
 278 radicals; the Kramers theorem forbids such a gap [34]. Super-
 279 imposed on the data in Fig. 6 are simulations that assume a
 280 ferromagnetic coupling between the radical and the Tb^{III} ion on
 281 each molecule; details concerning these simulations, which as-
 282 sume an isotropic g factor of ~ 2.00 and just a single interaction
 283 parameter, are given in the following section. As can be seen,
 284 agreement between the experiment and simulation is excellent.

285 IV. DISCUSSION

286 The preceding experiments provide clear evidence that the
 287 EPR signals seen for compounds **1** and **2** can be attributed,

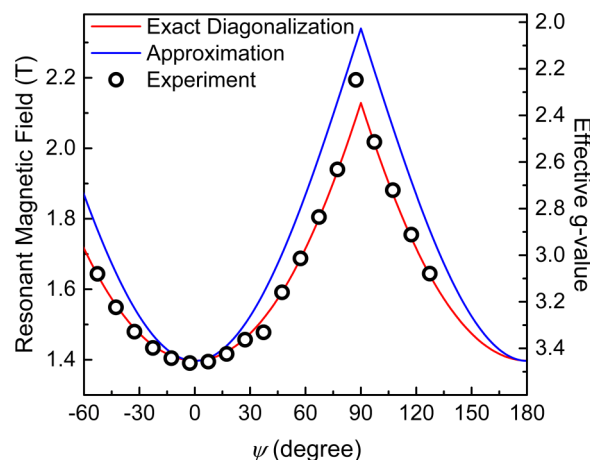


FIG. 5. Plot of the resonance positions in Fig. 3 [see also Fig. 4(a)], for one of the two molecular orientations; the polar coordinate has been transformed ($\theta \rightarrow \psi$) to a local frame, where $\psi = 0$ represents field parallel to the easy axis of the molecule. The solid curves represent two different simulations described in Sec. IV, one exact and the other approximate.

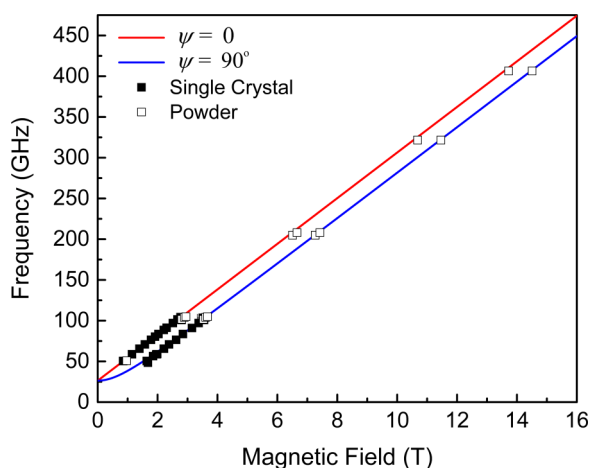


FIG. 6. Frequency versus magnetic field plot of the combined single-crystal (at $T = 2$ K) and powder (at $T = 5$ K) EPR data for **1**, with the field parallel ($\psi = 0^\circ$) and perpendicular ($\psi = 90^\circ$) to the easy axis of one of the molecular orientations; uncertainties in the determination of the resonance positions lie within the data points. The solid lines represent simulations described in Sec. IV.

to zeroth order, to the unpaired spin- $\frac{1}{2}$ on the Pc_2 radical. We now consider the source of considerable anisotropy of the radical signal in **1**. While rare, EPR spectra exhibiting similar degrees of anisotropy have been reported for crystals of magnetically ordered organic radical ferromagnets [35,36]. However, a smooth first-order angle dependence ($\sim \sin^2 \psi$) is observed in these cases, as opposed to the cusplike behavior observed at $\psi = 90^\circ$ in **1**. Moreover, the isotropic signal observed for **2** would also seem to rule out the possibility that long-range ordering of the radicals is responsible for the anisotropy in **1**. Hence coupling to the highly anisotropic Tb^{III} ion represents the obvious starting point for an analysis of the results.

We thus consider the simplest possible effective spin Hamiltonian of Eq. (1) that includes an isotropic (scalar) coupling between the radical and Ln moments, while absorbing all of the anisotropy into the zero-field-splitting (ZFS) Hamiltonian, $\hat{H}_{\text{ZFS}}^{\text{Tb}}$, of the terbium ion:

$$\hat{H}^{\text{eff}} = \hat{H}_{\text{ZFS}}^{\text{Tb}} + J_{\text{ex}} \hat{S}^{\text{rad}} \cdot \hat{J}^{\text{Tb}} + \hat{H}_Z^{\text{Tb}} + \hat{H}_Z^{\text{rad}}. \quad (1)$$

Here, \hat{S}^{rad} and \hat{J}^{Tb} , respectively, represent angular momentum operators associated with the radical (spin) and the lanthanide (spin orbital), while J_{ex} parametrizes the scalar coupling between them. Meanwhile, we assume isotropic Zeeman interactions, $\hat{H}_Z^{\text{Tb}} (= g_J \mu_B \vec{B}_0 \cdot \hat{J}^{\text{Tb}})$ and $\hat{H}_Z^{\text{rad}} (= g_e \mu_B \vec{B}_0 \cdot \hat{S}^{\text{rad}})$, with $g_e (= 2.00)$ and $g_J (= \frac{3}{2}$ for $\text{Tb}^{\text{III}})$ representing the Landé factors, and \vec{B}_0 the applied magnetic field.

The anisotropic ZFS interaction of the Tb^{III} ion can be expressed in terms of extended Stevens operators [37]:

$$\hat{H}_{\text{ZFS}}^{\text{Tb}} = \sum_{k=2,4,6} \sum_{q=-k}^k B_k^q \hat{O}_k^q. \quad (2)$$

The \hat{O}_k^q terms are comprised of angular momentum operators of rank k , which are then parametrized by their

accompanying B_k^q coefficients. The off-diagonal ($q \neq 0$) terms can be neglected for the purposes of this analysis, as they are known to influence the magnetic behavior of the Tb ion only at very low applied magnetic fields ($B_0 < 0.04$ T) [25]. This leaves only the cylindrically symmetric terms, $B_k^0 \hat{O}_k^0$ ($k = 2, 4, 6$), containing only even powers of the z -component angular momentum operator, \hat{J}_z^k , where we have dropped the ‘‘Tb’’ superscript here for compactness. In principle, the B_k^0 coefficients are known from thermodynamic measurements [24,25]. However, we find that the results of the simulations are completely insensitive to these parameters provided they are chosen so that the $m_J = \pm 6$ substates lie lowest in energy and are well separated from the first excited state, as is known to be the case experimentally. For these purposes, one can simplify the analysis greatly by retaining only the leading term $B_2^0 \hat{O}_2^0 = \{3\hat{J}_z^2 - \hat{J}(\hat{J} + 1)\}$, so long as the B_2^0 parameter is chosen to be negative and sufficiently large so that the Tb^{III} ZFS interaction dwarfs the remaining interactions in Eq. (1); i.e., the EPR measurements do not constrain this parameter (or any of the Tb^{III} ZFS parameters) [38].

The approach outlined above leaves J_{ex} , the scalar coupling, as the only free parameter in the model. The simulations in Figs. 5 and 6 assume a ferromagnetic interaction, $J_{\text{ex}} = -0.147 \text{ cm}^{-1}$. It is now relatively straightforward to understand the experimental observations within the context of this relatively simple model. In zero field, the radical is coupled only to the Tb^{III} ion, with doubly degenerate eigenstates $|+6, +\frac{1}{2}\rangle$, $|-6, -\frac{1}{2}\rangle$, and $|+6, -\frac{1}{2}\rangle$, $|-6, +\frac{1}{2}\rangle$, employing here an $|m_J, m_S\rangle$ representation. The energy separation between these states, $\Delta_0 = |6J_{\text{ex}}| = 0.88 \text{ cm}^{-1}$ or 26.4 GHz , corresponds to the zero-field gap in the EPR spectrum (see Fig. 6); as can be seen, the transitions $|+6, +\frac{1}{2}\rangle$ to $|+6, -\frac{1}{2}\rangle$ and $|-6, -\frac{1}{2}\rangle$ to $|-6, +\frac{1}{2}\rangle$ involve a simple spin flip of the radical under an exchange bias field due to the Tb^{III} ion; i.e., the gap corresponds to the energy difference between the ferromagnetic (F) and antiferromagnetic (A) configurations (meaning up/up and up/down, not to be confused here with long-range ordered states).

We next consider the field dependence of the EPR spectrum. Because of the strong crystal-field anisotropy of the Tb^{III} ion, it may be treated as an Ising-like moment; i.e., $\langle \hat{J}_x^{\text{Tb}} \rangle = \langle \hat{J}_y^{\text{Tb}} \rangle = 0$. Consequently, from a semiclassical point of view, the Tb^{III} moment is constrained along $\pm z$, the C_4 symmetry axis of the molecule (or $\psi = 0^\circ$). Meanwhile, in the intermediate field regime, the radical spin follows B_0 ; here, ‘‘intermediate’’ implies that the radical Zeeman interaction, \hat{H}_Z^{rad} , is strong enough to overcome the scalar coupling (i.e., $g_e \mu_B B_0 > \Delta_0$), but that the field is not yet so strong that it can compete with $\hat{H}_{\text{ZFS}}^{\text{Tb}}$. The scalar interaction energy then takes the form

$$J_{\text{ex}} \hat{S}^{\text{rad}} \cdot \hat{J}^{\text{Tb}} \approx \pm J_{\text{ex}} \left| \frac{1}{2} \frac{\vec{B}_0}{B_0} \cdot 6\hat{z} \right| = \pm 3 |J_{\text{ex}} \cos \psi|, \quad (3)$$

where the \pm signs denotes the F (–) and A (+) cases. Likewise, in this same intermediate field regime, the radical and Tb^{III} Zeeman interactions may be written

$$\begin{aligned} \hat{H}_Z^{\text{Tb}} &\approx \pm \frac{3}{2} \mu_B |\vec{B}_0 \cdot 6\hat{z}| = \pm 9 \mu_B B_0 |\cos \psi|, \\ \hat{H}_Z^{\text{rad}} &\approx \pm \mu_B B_0. \end{aligned} \quad (4)$$

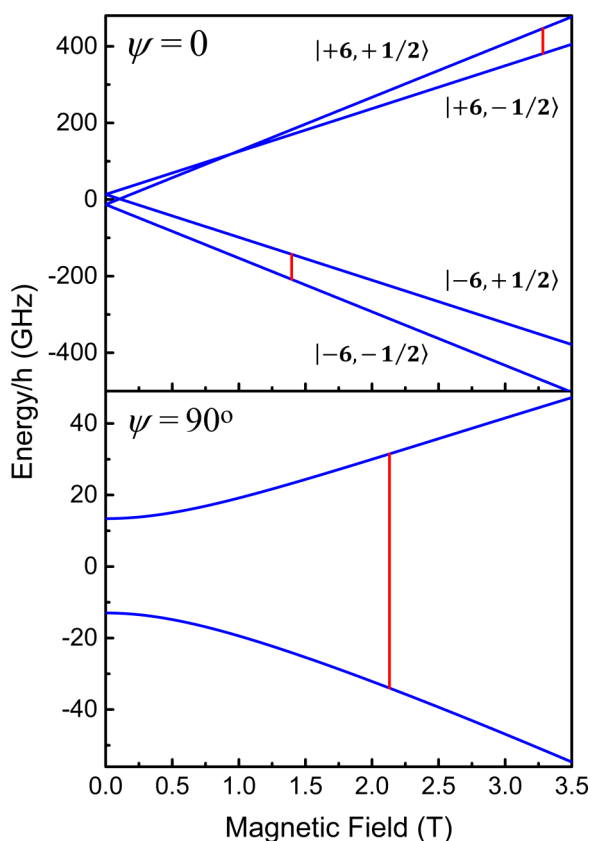


FIG. 7. Exact solutions to Eq. (1) with the field applied parallel (a) and perpendicular (b) to the easy axis of the $[\text{TbPC}_2]^0$ molecule; note that each of the solutions in (b) is doubly degenerate. The red lines denote allowed EPR transitions at 65.5 GHz, corresponding to a spin-flip of the radical.

370 The absolute value of the cosine recognizes the time-
 371 reversal invariance of the leading axial interaction, $\hat{H}_{\text{ZFS}}^{\text{Tb}}$, which
 372 means that the physics is the same regardless of whether the
 373 field is applied above or below the molecular hard plane.
 374 One can then write down expressions for the four energy
 375 eigenvalues, referenced to the uncoupled zero-field ground-
 376 state energy:

$$\begin{aligned} \epsilon_{0\pm} &\approx -|3J_{\text{ex}} \cos \psi| \pm 9\mu_B B_0 |\cos \psi| \pm \mu_B B_0, \\ \epsilon_{1\mp} &\approx +|3J_{\text{ex}} \cos \psi| \pm 9\mu_B B_0 |\cos \psi| \mp \mu_B B_0, \end{aligned} \quad (5)$$

377 where ϵ_0 and ϵ_1 correspond to the F and A cases, respectively
 378 (see Fig. 7); the inverted \mp in the second expression reflects
 379 the A coupling, i.e., the radical is “down” when the Tb^{III} is
 380 “up.” Radical EPR transitions involve a change in the sign of
 381 the last terms in Eq. (5), but no change in the second terms (the
 382 Tb^{III} Zeeman energy). The ground-state transition, $\epsilon_{0-} \rightarrow \epsilon_{1+}$,
 383 thus involves an energy,

$$\Delta\epsilon_0 \approx |6J_{\text{ex}} \cos \psi| + 2\mu_B B_0. \quad (6)$$

384 Although Eqs. (3)–(6) are approximate, they become exact
 385 for $\psi = 0^\circ$, because the Hamiltonian of Eq. (1) is diagonal in
 386 this limit. Therefore, $\Delta\epsilon_0 = \Delta_0 + 2\mu_B B_0$ for this orientation;
 387 i.e., the unperturbed transition energy ($g_e \mu_B B_0$, with $g_e =$
 388 2.00) for the radical is offset vertically by the zero-field gap,
 389

$\Delta_0 = |6J_{\text{ex}}|$, exactly as observed in Fig. 6. Meanwhile, for
 390 $\psi = 90^\circ$, the scalar coupling and Tb^{III} Zeeman interactions
 391 are identically zero in the intermediate field regime (because
 392 $\hat{S}^{\text{rad}} \cdot \hat{J}^{\text{Tb}} = \hat{B}_0 \cdot \hat{J}^{\text{Tb}} = 0$), resulting in an EPR spectrum that
 393 is indistinguishable from that of an isolated radical, i.e., a $g_e =$
 394 2.00 resonance with no zero-field offset, again in reasonable
 395 agreement with experiment (Fig. 6).
 396

The overall effect of the scalar coupling is to shift the
 397 ground-state EPR positions by an amount
 398

$$\Delta B_0 \approx - \left| \frac{3J_{\text{ex}} \cos \psi}{\mu_B} \right|, \quad (7)$$

below the isotropic $g = 2.00$ position (~ 2.34 T at 65.5 GHz),
 399 where $|3J_{\text{ex}}/\mu_B| \approx 0.94$ T. Here, one sees the reason for the
 400 cusplike turning point of the resonance position at $\psi = 90^\circ$
 401 and the broad minimum at $\psi = 0^\circ$ (Fig. 5). The experimental
 402 downshift of 0.94 T to 1.4 T at $\psi = 0^\circ$ is in excellent agreement
 403 with experiment. However, the angle-dependent data presented
 404 in Fig. 5 were obtained slightly below the “intermediate” field
 405 regime, so that the approximation does not work as well when
 406 the field rotates away from $\psi = 0^\circ$. The scalar interaction
 407 dominates at low fields, meaning that there is a residual
 408 coupling to the Tb^{III} ion even at $\psi = 90^\circ$, thus explaining
 409 why the resonance occurs slightly below the $g = 2.00$ position.
 410 Indeed, this is also the reason why Eq. (7) does not account
 411 quantitatively for the experimental results in Fig. 5 quite as well
 412 as the simulations involving exact diagonalization of Eq. (1);
 413 comparisons between the exact and approximate expressions
 414 at much higher fields do give near perfect agreement.
 415

For the magnetic fields (> 1 T) and temperatures (~ 2 K) at
 416 which the experiments were carried out, only the $|-6, -\frac{1}{2}\rangle$ (at
 417 ϵ_{0-}) and $|-6, +\frac{1}{2}\rangle$ (at ϵ_{1+}) states are significantly populated
 418 when the applied field has an appreciable component along
 419 z ; this is because of the strong Zeeman interaction associated
 420 with the Tb^{III} ion ($\pm 9\mu_B B_0 |\cos \psi|$). Hence only the ground-
 421 state EPR transition is observed for most field orientations.
 422 However, this is not necessarily the case when ψ is close to 90° .
 423 In fact, the $\epsilon_{0\pm}$ and $\epsilon_{1\mp}$ states are quasidegenerate at exactly
 424 $\psi = 90^\circ$, because the radical EPR transition is insensitive to
 425 the state of the Tb^{III} ion, which lives in a nonmagnetic superpo-
 426 sition of the $m_J = \pm 6$ states (with a minuscule tunneling gap
 427 on the order of kHz) [25]. Thus one may think of two (quasi-)
 428 degenerate radical EPR transitions, one for each of the Tb^{III}
 429 degrees of freedom. Meanwhile, slightly away from $\psi = 90^\circ$,
 430 this degeneracy is lifted because of the weak longitudinal
 431 ($//z$) field component, yet both transitions may be expected
 432 to possess detectable Boltzmann weights, thereby explaining
 433 the observation of an additional peak at some orientations close
 434 to $\psi = 90^\circ$ in Fig. 3 (indicated by *). However, the intensity
 435 of the higher-lying transition will rapidly lose weight as the
 436 field rotates away from $\psi = 90^\circ$.
 437

It is natural to question the validity of such a simple
 438 model [Eq. (1)]. In particular, why assume a scalar coupling?
 439 Exchange involving spin-orbital moments only couples the
 440 spin part of the wave function and, for instance, in Ref. [12],
 441 we have expressed this Heisenberg interaction as $J_{\text{ex}} \hat{S}^{\text{rad}} \cdot \hat{S}^{\text{Tb}}$.
 442 However, our choice here does not alter the underlying physics,
 443 because \hat{L} is strongly coupled to \hat{S} , and the net effect would
 444 simply be a renormalization of the coupling parameter, J_{ex} ,
 445

446 doubling its value in the case of Tb^{III} . Similarly, why not
 447 consider an anisotropic coupling, such as an Ising or dipolar
 448 interaction? The Ising character is already built into the model
 449 via the ZFS interaction associated with the Tb^{III} ion. An
 450 anisotropic coupling (\vec{J}_{ex} is now a tensor) would simply add su-
 451 perfluous parameters. We note that recent CASSCF (complete
 452 active space self-consistent field) *ab initio* calculations [12,39]
 453 on $[\text{TbPc}_2]^0$ using a minimal active space of $4f$ orbitals and the
 454 π -ligand singly occupied molecular orbital (π -SOMO), also
 455 including spin-orbit coupling nonperturbatively, fully support
 456 our current assumption that the radical- $4f$ exchange coupling
 457 is (i) much smaller than the gap between ground and first
 458 excited crystal-field substates; and (ii) well described by an
 459 isotropic exchange Hamiltonian.

460 Another potential source of anisotropic coupling that should
 461 be considered is the purely through-space dipolar interaction
 462 between the Tb^{III} ion and the spin density on the radical, which
 463 can in principle be calculated precisely via *ab initio* methods.
 464 However, one can also get a good sense for the magnitude of
 465 this interaction by assuming that the radical spin density is
 466 localized on the C and N atoms of the ligand, and then perform
 467 simple point-dipole calculations. Published density functional
 468 theory (DFT) results suggest that most of the spin density
 469 resides on the 16 inner C atoms (on average $0.05 \mu_{\text{B}}/\text{C}$), which
 470 are located at an average distance of 3.33 \AA from the Tb^{III}
 471 ion [17]. Meanwhile, the remainder of the density resides
 472 on the 48 C atoms of the outer rings ($0.005 \mu_{\text{B}}/\text{C}$), with a
 473 small negative polarization on the 16 coordinating N atoms
 474 (about $-0.01 \mu_{\text{B}}/\text{N}$). Interestingly, based on a point-dipole
 475 approximation, we find the coupling to be antiferromagnetic
 476 for nearly all of these sites. The closest eight N atoms sit
 477 at an average angle of 54.55° from the Tb ion, as measured
 478 from the C_4 axis of the molecule. This is fractionally below
 479 the magic angle of $\psi_m = 54.7^\circ$ [$3\cos^2\psi_m - 1 = 0$], meaning
 480 that the contribution of these sites to the dipolar interaction is
 481 near negligible because of the axial symmetry of the molecule.
 482 Moreover, because the polarization is negative at these sites,
 483 their contribution to the coupling will be antiferromagnetic.
 484 The remaining atoms all sit at angles beyond ψ_m . Therefore,
 485 the remaining eight N atoms provide the only ferromagnetic
 486 coupling. However, this contribution is overwhelmed by the
 487 carbon atoms, which all couple antiferromagnetically to the
 488 Tb^{III} ion. A weighted sum of point-dipolar contributions gives
 489 an estimate for the ZFS of $\Delta_0 \approx 1.3 \text{ GHz}$, corresponding to a
 490 $J_{\text{ex}} = +7.2 \times 10^{-3} \text{ cm}^{-1}$. Thus not only is the sign incorrect,
 491 but the magnitude of the coupling is more than an order of
 492 magnitude too small. Therefore, the main contribution to the
 493 coupling has to involve exchange, and Eq. (1) is expected to
 494 capture the essential physics.

495 There have been a limited number of previous (and
 496 conflicting) experimental and theoretical attempts to eval-
 497 uate the radical-lanthanide exchange interaction in bis-
 498 phthalocyaninato-type Ln complexes. The earliest study on
 499 $[\text{LnPc}_2]^0$ suggested a strong antiferromagnetic coupling (when
 500 $\text{Ln} = \text{Gd}, \text{Tb}, \text{Ho}$) on the basis of relatively high-temperature
 501 magnetic susceptibility measurements [18,19]. More recently,
 502 both ferro- and antiferromagnetic interactions have been de-
 503 duced from single-molecule transistor experiments [15,17],
 504 although a large anisotropic exchange term (amounting to 60%

505 of the isotropic component) was introduced in Ref. [17] in
 506 order to explain some features of the observed Kondo reso-
 507 nance. Meanwhile, recent NMR/DFT studies on a $[\text{TbPc}_2]^0$
 508 complex very similar to the one studied here have suggested
 509 ferromagnetic coupling due to the orthogonality between the
 510 broken-symmetry ligand-centered π -SOMO and the seven $4f$
 511 magnetic orbitals with opposite spin polarization [40]. We
 512 note, however, that the energies of the high- and low-spin
 513 states of $[\text{GdPc}_2]^0$ were not reported in Ref. [39], so it is
 514 difficult to assess whether other exchange mechanisms (e.g.,
 515 spin polarization) could stabilize an antiferromagnetic ground
 516 state, despite the orthogonality between magnetic orbitals.
 517 Another quite recent DFT calculation shows that the exchange
 518 coupling between the f electrons and the radical is mediated by
 519 d electrons of the Tb^{III} ion that significantly overlap the N and
 520 C orbitals of the Pc ligands and, due to large spin-polarization
 521 effects, lead to antiferromagnetic coupling [11]. Meanwhile,
 522 combined XMCD, CASSCF/RASSI-SO, and DFT studies of
 523 $[\text{TbPc}_2]^0$ grafted onto surfaces point to ferromagnetic coupling
 524 [12], although the results depend on the details of the modeling
 525 and are sensitive to molecule configuration.

526 The present EPR experiments undoubtedly demonstrate
 527 a ferromagnetic Tb-radical exchange interaction in the bulk
 528 $[\text{TbPc}_2]^0$ derivative crystallized in the $Pnma$ space group. One
 529 may actually expect such coupling on the basis of relatively
 530 simple molecular point group symmetry considerations [38]. It
 531 turns out that, for exact molecular D_{4d} symmetry, the π -SOMO
 532 (ϕ_π) on the Pc_2 ligand system spans a $\Gamma_\pi = a_2$ irreducible
 533 representation of D_{4d} , while the irreducible representations
 534 spanned by the $4f$ orbitals of the central Tb^{III} ion are $\Gamma_{4f} =$
 535 $b_2 + e_1 + e_2 + e_3$ [38]. Therefore, the kinetic contribution
 536 to the exchange, proportional to the matrix element of a
 537 totally symmetric Hamiltonian, h , inducing virtual transitions
 538 between the π -SOMO and the Tb $4f$ atomic orbitals, is clearly
 539 zero by symmetry, i.e., $\langle \phi_\pi | h | 4f \rangle = 0$, since $\Gamma_\pi \times \Gamma_{4f}$ does
 540 not include the totally symmetric irreducible representation. It
 541 is this contribution that favors antiferromagnetic coupling [34].
 542 Therefore, its absence leaves only potential exchange within
 543 the restricted excitation space of the π -SOMO and seven $4f$ or-
 544 bitals. This interaction is given by the exchange integral, which
 545 is always ferromagnetic and necessarily isotropic. Considera-
 546 tion of extended excitation spaces may introduce additional
 547 (likely weaker) terms, both isotropic and anisotropic, and of
 548 either sign [34,38]. However, the simple symmetry arguments
 549 presented here seem to confirm the ferromagnetic coupling that
 550 is found experimentally.

551 Finally, Branzoli *et al.* reported an antiferromagnetic in-
 552 termolecular exchange interaction between $[\text{YPc}_2]^0$ radicals
 553 (here, Y is nonmagnetic) from magnetization, ^1He NMR
 554 paramagnetic shifts, and NMR T_1 measurements [41]. Mean-
 555 while, specific heat measurements on LnPc_2 ($\text{Ln} = \text{Y}, \text{Tb}$)
 556 also evidence the presence of extended spin excitations at
 557 low temperature [42]. Effects of such intermolecular interac-
 558 tions are not evident in the single-crystal EPR measurements
 559 presented here; in particular, the observation of independent
 560 (noninteracting) signals for the two molecular orientations
 561 would seem to rule this out. However, weak satellite peaks
 562 observed in the powder measurements ($\sim 0.15 \text{ T}$ above and
 563 below the strong low-field resonance in Fig. 1) at the low-
 564 est temperatures, may provide evidence for intermolecular

565 interactions in the $P2_12_12_1$ structure (γ phase). These satellite
566 peaks have no counterpart in the single-crystal EPR measure-
567 ments. However, x-ray structure studies of the powder sample
568 employed in this study suggest a small contamination with the
569 $P2_12_12_1$ phase. Future work aims to address the issue of inter-
570 molecular exchange interactions in $\text{Ln}(\text{Pc})_2$ crystals in more
571 detail.

572 V. CONCLUSIONS

573 We present detailed high-field, high-frequency EPR mea-
574 surements on a powder and a single-crystal sample of a
575 previously unreported structural phase ($Pnma$ space group) of
576 the neutral terbium bis-phthalocyaninato metalorganic com-
577 plex, $[\text{TbPc}_2]^0$. An anisotropic EPR spectrum is observed,
578 which is attributed to the $s = \frac{1}{2}$ radical delocalized over the
579 Pc_2 ligand. The magnetic anisotropy results from a weak
580 coupling of the radical to the Ising-like spin-orbital moment
581 of the Tb^{III} ion. Angle-dependent EPR studies reveal two
582 differently oriented, magnetically independent molecules, in
583 agreement with x-ray structural studies. Analyses of the results
584 unambiguously demonstrate that the radical- Tb^{III} coupling is
585 due to a ferromagnetic exchange interaction. The essential
586 physics is captured via an effective spin Hamiltonian in which
587 the exchange is assumed to be isotropic ($J_{\text{ex}} = -0.147 \text{ cm}^{-1}$),

while the magnetic anisotropy is folded entirely into the single- 588
ion properties of the Tb^{III} ion. This model is rationalized on 589
the basis of the simple symmetry considerations that dictate 590
an orthogonality of the Tb $4f$ orbitals and the π -SOMO 591
associated with the Pc_2 ligand, thereby suppressing virtual 592
hopping transitions that mediate antiferromagnetic exchange 593
interactions. 594

ACKNOWLEDGMENTS

We acknowledge financial support from the **US National** 596
Science Foundation (Grant No. **DMR-1610226**), the **Air Force** 597
Office of Scientific Research (**Asian Office of Research and** 598
Development, Contract No. **FA2386-17-1-4040**), the **Italian** 599
Ministry of Education and Research (MIUR) through the PRIN 600
Project No. **2015HYFSRT**, the **DFG-TR 88** “3Met,” and **ANR-** 601
13-BS10-0001-03 MolQuSpin. A.S. and M.A. acknowledge 602
financial support from the **Australian Research Council**, Dis- 603
covery Grant No. **DP15010325**. A portion of this work was 604
performed at the U.S. National High Magnetic Field Labora- 605
tory, which is supported by the **National Science Foundation** 606
(Grant No. **DMR-1157490**) and the State of Florida. We 607
also acknowledge the Karlsruhe Nano Micro Facility (KNMF, 608
www.kit.edu/knmf) for providing access to instruments at their 609
laboratories. 610

-
- [1] K. L. M. Harriman, A. A. Leitch, S. A. Stoian, F. Habib, J. L. Kneebone, S. I. Gorelsky, I. Korobkov, S. Desgreniers, M. L. Neidig, S. Hill, M. Murugesu, and J. L. Brusso, Ambivalent binding between a radical-based pincer ligand and iron, *Dalton Trans.* **44**, 10516 (2015).
- [2] E. C. Constable, 2, 2':6', 2''-Terpyridines: From chemical obscurity to common supramolecular motifs, *Chem. Soc. Rev.* **36**, 246 (2007).
- [3] E. A. Medlycott and G. S. Hanan, Designing tridentate ligands for ruthenium(II) complexes with prolonged room temperature luminescence lifetimes, *Chem. Soc. Rev.* **34**, 133 (2005).
- [4] R. Shunmugam, G. J. Gabriel, K. A. Aamer, and G. N. Tew, Metal-ligand-containing polymers: Terpyridine as the supramolecular unit, *Macromol. Rapid Commun.* **31**, 784 (2010).
- [5] C. Benelli, A. Caneschi, D. Gatteschi, and R. Sessoli, Magnetic interactions and magnetic ordering in rare earth metal nitronyl nitroxide chains, *Inorg. Chem.* **32**, 4797 (1993).
- [6] L. Bogani, C. Sangregorio, R. Sessoli, and D. Gatteschi, Molecular engineering for single-chain-magnet behavior in a one-dimensional dysprosium-nitronyl nitroxide compound, *Angew. Chem., Int. Ed.* **44**, 5817 (2005).
- [7] K. Bernot, L. Bogani, A. Caneschi, D. Gatteschi, and R. Sessoli, A family of rare-earth-based single chain magnets: Playing with anisotropy, *J. Am. Chem. Soc.* **128**, 7947 (2006).
- [8] W. J. Evans, D. S. Lee, D. B. Rego, J. M. Perotti, S. A. Kozimor, E. K. Moore, and J. W. Ziller, Expanding dinitrogen reduction chemistry to trivalent lanthanides via the LnZ_3 /alkali metal reduction system: Evaluation of the generality of forming $\text{Ln}_2(\mu-\eta^2 : \eta^2-\text{N}_2)$ complexes via LnZ_3/K , *J. Am. Chem. Soc.* **126**, 14574 (2004).
- [9] J. D. Rinehart, M. Fang, W. J. Evans, and J. R. Long, A N_2^{3-} radical-bridged terbium complex exhibiting magnetic hysteresis at 14 K, *J. Am. Chem. Soc.* **133**, 14236 (2011).
- [10] J. D. Rinehart, M. Fang, W. J. Evans, and J. R. Long, Strong exchange and magnetic blocking in N_2^{3-} -radical-bridged lanthanide complexes, *Nat. Chem.* **3**, 538 (2011).
- [11] A. Candini, D. Klar, S. Marocchi, V. Corradini, R. Biagi, V. De Renzi, U. del Pennino, F. Troiani, V. Bellini, S. Klyatskaya, M. Ruben, K. Kummer, N. B. Brookes, H. Huang, A. Soncini, H. Wende, and M. Affronte, Spin-communication channels between $\text{Ln}(\text{III})$ bis-phthalocyanines molecular nanomagnets and a magnetic substrate, *Sci. Rep.* **6**, 21740 (2016).
- [12] S. Marocchi, A. Candini, D. Klar, W. Van Den Heuvel, H. Huang, F. Troiani, V. Corradini, R. Biagi, V. De Renzi, S. Klyatskaya, K. Kummer, N. B. Brookes, M. Ruben, H. Wende, U. Del Pennino, A. Soncini, M. Affronte, and V. Bellini, Relay-like exchange mechanism through a spin radical between TbPc_2 molecules and graphene/ $\text{Ni}(111)$ substrates, *ACS Nano* **10**, 9353 (2016).
- [13] A. Candini, S. Klyatskaya, M. Ruben, W. Wernsdorfer and M. Affronte, Graphene spintronic devices with molecular nanomagnets, *Nano Lett.* **11**, 2634 (2011).
- [14] M. Urdampilleta, S. Klyatskaya, M. Ruben, and W. Wernsdorfer, Magnetic interaction between a radical spin and a single-molecule magnet in a molecular spin-valve, *ACS Nano* **9**, 4458 (2015).
- [15] R. Vincent, S. Klyatskaya, M. Ruben, W. Wernsdorfer, and F. Balestro, Electronic read-out of a single nuclear spin using a molecular spin transistor, *Nature* **488**, 357 (2012).
- [16] S. Thiele, F. Balestro, R. Ballou, S. Klyatskaya, M. Ruben, and W. Wernsdorfer, Electrically driven nuclear spin resonance in single-molecule magnets, *Science* **344**, 1135 (2014).

- [17] C. Godfrin, S. Thiele, A. Ferhat, S. Klyatskaya, M. Ruben, W. Wernsdorfer, and F. Balestro, Electrical read-out of a single spin using an exchange-coupled quantum dot, *ACS Nano* **11**, 3984 (2017).
- [18] K. L. Trojan, W. E. Hatfield, K. D. Kepler, and M. L. Kirk, Strong exchange coupling in lanthanide bis-(phthalocyaninato) sandwich compounds, *J. Appl. Phys.* **69**, 6007 (1991).
- [19] K. L. Trojan, J. L. Kendall, K. D. Kepler, and W. E. Hatfield, Strong exchange coupling between the lanthanide ions and the phthalocyaninato ligand radical in bis(phthalocyaninato)lanthanide sandwich compounds, *Inorg. Chim. Acta* **198-200**, 795 (1992).
- [20] T. Ishida, T. Nakamura, T. Kihara, and H. Nojiri, Chemical trend on the lanthanide-radical exchange coupling, *Polyhedron* **136**, 149 (2017).
- [21] M. L. Baker, T. Tanaka, R. Murakami, S. Ohira-Kawamura, K. Nakajima, T. Ishida, and H. Nojiri, Relationship between torsion and anisotropic exchange coupling in a Tb^{III}-radical-based single-molecule magnet, *Inorg. Chem.* **54**, 5732 (2015).
- [22] N. Ishikawa, M. Sugita, T. Ishikawa, S. Y. Koshihara, and Y. Kaizu, Lanthanide double-decker complexes functioning as magnets at the single-molecular level, *J. Am. Chem. Soc.* **125**, 8694 (2003).
- [23] N. Ishikawa, M. Sugita, N. Tanaka, T. Ishikawa, S. Y. Koshihara, and Y. Kaizu, Upward temperature shift of the intrinsic phase lag of the magnetization of bis(phthalocyaninato)terbium by ligand oxidation creating an $S = \frac{1}{2}$ spin, *Inorg. Chem.* **43**, 5498 (2004).
- [24] N. Ishikawa, M. Sugita, T. Okubo, N. Tanaka, T. Iino, and Y. Kaizu, Determination of ligand-field parameters and f-electronic structures of double-decker bis(phthalocyaninato)-lanthanide complexes, *Inorg. Chem.* **42**, 2440 (2003).
- [25] N. Ishikawa, M. Sugita, and W. Wernsdorfer, Quantum tunneling of magnetization in lanthanide single-molecule magnets: Bis(phthalocyaninato)terbium and bis(phthalocyaninato)dysprosium anions, *Angew. Chem., Int. Ed.* **44**, 2931 (2005).
- [26] M. Shiddiq, D. Komijani, Y. Duan, A. Gaita-Ariño, E. Coronado, and S. Hill, Enhancing coherence in molecular spin qubits via atomic clock transitions, *Nature* **531**, 348 (2016).
- [27] F. Branzoli, P. Carretta, M. Filibian, M. J. Graf, S. Klyatskaya, M. Ruben, F. Coneri, and P. Dhakal, Spin and charge dynamics in [TbPc₂]⁰ and [DyPc₂]⁰ single-molecule magnets, *Phys. Rev. B* **82**, 134401 (2010).
- [28] A. Hassan, L. Pardi, J. Krzystek, A. Sienkiewicz, P. Goy, M. Rohrer, and L.-C. Brunel, Ultrawide band multifrequency high-field EMR technique: A methodology for increasing spectroscopic information, *J. Magn. Reson.* **142**, 300 (2000).
- [29] M. Mola, S. Hill, P. Goy, and M. Gross, Instrumentation for millimeter-wave magnetoelectrodynamic investigations of low-dimensional conductors and superconductors, *Rev. Sci. Instrum.* **71**, 186 (2000).
- [30] S. Takahashi and S. Hill, Rotating cavity for high-field angle-dependent microwave spectroscopy of low-dimensional conductors and magnets, *Rev. Sci. Instrum.* **76**, 23114 (2005).
- [31] S. Stoll and A. Schweiger, EasySpin, a comprehensive software package for spectral simulation and analysis in EPR, *J. Magn. Reson.* **178**, 42 (2006).
- [32] See Supplemental Material at <http://link.aps.org/supplemental/10.1103/PhysRevMaterials.xx.xxxxx> for crystal structures in CIF format.
- [33] C. Loosli, S.-X. Liu, A. Neels, G. Labat, and S. Decurtins, Crystal structures of tetrabutylammonium bis(phthalocyaninato)terbium(III) methanol solvate hydrate (1:1:3/2), [N(C₄H₉)₄][Tb(C₈H₄N₂)₂] · CH₃OH · 3/2H₂O, and tetrabutylammonium bis(phthalocyaninato)dysprosium(III) methanol solvate hydrate (1:1:1), [N(C₄H₉)₄][Dy(C₈H₄N₂)₂] · CH₃OH · H₂O, *Z. Kristallogr. -New Cryst. Struct.* **221**, 135 (2006).
- [34] H. A. Kramers, General theory of paramagnetic rotation in crystals, *Proc. Amsterdam Acad.* **33**, 959 (1930).
- [35] S. M. Winter, S. Hill, and R. T. Oakley, Magnetic ordering and anisotropy in heavy atom radicals, *J. Am. Chem. Soc.* **137**, 3720 (2015).
- [36] S. M. Winter, R. T. Oakley, A. Kovalev, and S. Hill, Spin-orbit effects in heavy-atom organic radical ferromagnets, *Phys. Rev. B* **85**, 094430 (2012).
- [37] K. W. H. Stevens, Matrix elements and operator equivalents connected with the magnetic properties of rare earth ions, *Proc. Phys. Soc., London, Sect. A* **65**, 209 (1952).
- [38] S. Ghosh, S. Datta, L. Friend, S. Cardona-Serra, A. Gaita-Ariño, E. Coronado, and S. Hill, Multi-frequency EPR studies of a mononuclear holmium single-molecule magnet based on the polyoxometalate [Ho^{III}(W₅O₁₈)₂]⁹⁻, *Dalton Trans.* **41**, 13697 (2012).
- [39] H. Huang, W. Van den Heuvel, and A. Soncini, *Ab initio* multi-reference investigation of the exchange coupling between 4f-electrons and π -radical in [LnPc₂]⁰ molecules (unpublished).
- [40] M. Damjanovic, T. Morita, K. Katoh, M. Yamashita, and M. Enders, Ligand π -radical interaction with f-shell unpaired electrons in phthalocyaninato-lanthanoid single-molecule magnets: A solution NMR spectroscopic and DFT study, *Chem. - Eur. J.* **21**, 14421 (2015).
- [41] F. Branzoli, P. Carretta, M. Filibian, S. Klyatskaya, and M. Ruben, Low-energy spin dynamics in the [YPc₂]⁰ $S = \frac{1}{2}$ anti-ferromagnetic chain, *Phys. Rev. B* **83**, 174419 (2011).
- [42] A. Ghirri and M. Affronte (unpublished).